A&A manuscript no.
(will be inserted by hand later)

Your thesaurus codes are:
07(08.01.2; 08.19.6; 08.09.1; 08.09.2 V824 Ara; 08.12.1)

ASTRONOMY AND ASTROPHYSICS

February 1, 2000

Doppler imaging of stellar surface structure

XIV. The double-lined pre-main-sequence binary V824 Arae = HD 155555⋆

K. G. Strassmeier[1] **and J. B. Rice**[2]

[1] Institut für Astronomie, Universität Wien, Türkenschanzstraße 17, A-1180 Wien, Austria, strassmeier@astro.univie.ac.at
[2] Department of Physics, Brandon University, Brandon, Manitoba R7A 6A9, Canada, rice@BrandonU.ca

Received ... ; accepted ...

Abstract. Photospheric Doppler images for both stellar components of the double-lined pre-main-sequence binary V824 Ara reveal surface temperature inhomogeneities of up to 1800 K on both stars. The spot geometry on the hotter primary is dominated by an elongated, tilted, equatorial feature but our maps from two spectral regions consistently also show a polar spot cooler by 1700 K. The secondary star has spots mainly at low and very high latitudes but not a polar cap. A flux-tube simulation with appropriate stellar models for V824 Ara suggests that any polar or very high-latitude spot must have formed after flux-tube emergence. Generally, the low-latitude spots on both stellar components appear to be mostly concentrated on the hemispheres turned away from each other.

We present new radial velocities and use them to re-evaluate the orbital elements and to derive absolute parameters for both stellar components. The absolute brightness and mass of the two stars suggest that they are very close to the main sequence – but not yet on the ZAMS – if an inclination of the orbital plane (and rotational axes) of 52° is adopted as suggested by the Doppler imaging. Since both stars are active, we solve for the inclinations of both stellar components separately and find that the values agree to within their uncertainties.

Key words: stars: activity of – starspots – stars: imaging – stars: individual: V824 Ara – stars: late-type

1. The V824-Ara system

V824 Ara (HD 155555, V=$6\overset{\mathrm{m}}{.}9$) consists of a G5 IV primary star and a K0 IV-V secondary star in a short-period orbit of $P = 1.68$ days. It is listed as a RS CVn binary in the "chromospherically active binary star" (CABS) catalog (Strassmeier et al. 1993) but its inclusion is simply based on activity and binarity, not on evolutionary status. The evolutionary status of V824 Ara – either evolved or pre-main sequence – is not completely clear despite relatively strong lithium lines from both components. Pasquini et al. (1991) suggested that the binary is part of the young disk population in agreement with the high Li I 6708-Å abundance. There is also a nearby M-star companion (LDS 587B) 33″ away. With this visual companion showing very high levels of activity and lithium abundance (Martin & Brandner 1995) it seems likely that the V824 Ara + LDS587B system is indeed a pre-main-sequence object. Strong Ca II H and K emission, filled-in Hα, and radio and X-ray emission (e.g. Dempsey et al. 1993) are also consistent with V824 Ara being an active, short-period binary system. Furthermore, the existence of highly ionized iron emission lines in the EUV spectrum, e.g. from Fe XXIII or Fe XX, indicate the existence of an extended hot corona (Dempsey et al. 1998).

A first Doppler image of the photosphere of the primary component of V824 Ara was presented by Kürster et al. (1992) and revealed a large, somewhat decentered, polar cap-like spot and possibly one smaller equatorial spot. Such large polar spots are common for the active post-main-sequence binaries of the RS CVn type, e.g. on V711 Tau (Vogt et al. 1999, Donati 1999, Strassmeier & Bartus 2000), EI Eri (Strassmeier et al. 1991), and many other targets in previous papers in this series. Prominent polar spots are also seen on active pre-main-sequence stars, e.g. on the weak-lined T Tauri's HDE 283572 (Strassmeier & Rice 1998, Joncour et al. 1994) and V410 Tau (e.g. Rice & Strassmeier 1996, Hatzes 1995), or on the classical T Tauri object Sz 68 (Johns-Krull & Hatzes 1997). Similar is reported for rapidly-rotating ZAMS stars like AB Dor (e.g. Collier-Cameron 1995), the young α Per-stars HE 699 and HE 520 (Barnes et al. 1998), and the low-mass Pleiades stars HII 686 and HII 3163 (Stout-Batalha & Vogt 1999).

The more detailed Doppler-imaging study of V824 Ara by Hatzes & Kürster (1999) from observations in 1990 confirmed the polar spot that was first detected by Kürster et al. (1992) from a preliminary report of the same observations. Hatzes & Kürster (1999) presented a first map of the secondary star and found a polar feature on it as well. As this polar spot was also decentered with respect to the stellar rotation pole, as on the primary star, and pointing towards each other, the authors tentatively suggested a possible link between the polar spot distribution and tidal forces.

In this paper, we present Doppler images for both components of V824 Ara from an independent set of spectra taken in May 1996. These data were obtained contemporaneously

⋆ Based on observations collected at the European Southern Observatory

Table 1. ESO-CAT radial velocities for the primary (S1) and secondary (S2) components of V824 Ara

HJD	Orbital	v_{S1}	(O-C)	v_{S2}	(O-C)
	Phase	($km\,s^{-1}$)			
2450221.795	0.8031	32.95	-1.1	-27.65	-2.6
2450221.856	0.8393	52.35	0.6	-46.79	-2.4
2450221.872	0.8489	57.21	1.2	-51.96	-2.8
2450221.888	0.8584	61.53	1.4	-57.62	-4.0
2450221.904	0.8679	64.85	0.8	-63.22	-5.3
2450221.919	0.8768	69.26	1.8	-68.18	-6.5
2450221.934	0.8857	72.95	2.2	-70.25	-4.9
2450222.677	0.3276	-35.80	-1.4	52.01	1.7
2450222.692	0.3365	-37.54	0.9	56.92	2.0
2450222.707	0.3454	-43.65	-1.0	61.99	2.6
2450222.722	0.3543	-47.61	-1.1	65.86	2.2
2450222.784	0.3912	-63.07	-2.3	83.31	4.0
2450222.844	0.4269	-71.11	0.0	92.67	1.9
2450222.859	0.4358	-73.02	0.1	95.47	2.5
2450222.874	0.4447	-74.09	0.8	97.20	2.3
2450222.889	0.4536	-75.68	0.7	98.49	1.9
2450222.914	0.4685	-77.33	1.0	100.33	1.6
2450222.929	0.4774	-78.59	0.6	100.95	1.3
2450223.683	0.9258	83.44	0.6	-80.51	-1.9
2450223.699	0.9353	89.94	4.9	-82.72	-1.8
2450223.716	0.9454	87.05	0.1	-82.28	0.8
2450223.732	0.9549	91.78	3.2	-85.34	-0.4
2450223.807	0.9995	94.09	2.1	-83.93	4.7
2450223.825	0.0102	92.24	0.4	-87.52	0.9
2450223.843	0.0209	91.60	0.3	-84.25	3.5
2450224.815	0.5989	-64.12	-0.1	85.69	2.8
2450224.830	0.6078	-62.09	-1.0	83.45	3.8
2450224.845	0.6168	-57.38	0.5	77.75	1.5
2450224.860	0.6257	-53.33	1.2	73.79	1.2
2450224.875	0.6346	-49.03	2.0	67.78	-0.9
2450224.890	0.6435	-44.63	2.7	62.05	-2.5
2450224.905	0.6524	-40.97	2.5	56.50	-3.8
2450224.919	0.6608	-36.41	3.3	51.91	-4.3
2450224.934	0.6697	-34.14	1.5	46.48	-5.2
2450225.677	0.1115	72.55	0.8	-64.63	1.7
2450225.692	0.1204	68.43	-0.0	-60.47	2.3
2450225.707	0.1294	65.32	0.2	-55.69	3.3
2450225.770	0.1668	47.57	-1.3	-36.12	5.1
2450225.785	0.1757	42.85	-1.7	-31.85	4.7
2450225.799	0.1841	37.66	-2.9	-26.12	6.0
2450226.853	0.8108	37.49	-0.5	-32.26	-2.9
2450226.868	0.8198	43.02	0.5	-37.57	-3.3
2450226.883	0.8287	47.18	0.4	-41.49	-2.5
2450226.898	0.8376	51.73	0.8	-46.53	-3.0
2450226.913	0.8465	56.69	1.7	-51.20	-3.2
2450226.927	0.8548	60.63	2.0	-56.22	-4.2
2450226.943	0.8644	64.31	1.7	-61.66	-5.3

to HST-GHRS, EUVE, and radio observations of V824 Ara (Dempsey et al. 1998). In a forthcoming paper, Dempsey et al. (2000) will relate our photospheric images to chromospheric and coronal diagnostics.

Table 2. Summary of optical photometry. $\Delta\lambda$ is the bandpass, Δt the time interval in days from JD 2,450,000, N is the number of nights, and n the number of datapoints,

Site	Observer	$\Delta\lambda$	Δt	N	n
SAAO	D. Kilkenny	UBVRI	197–214	7	62
MJUO	E. Budding	UBVRI	203–206	3	60
Waiharara	W. Walker	UBV	200–210	6	140
Auckland	H. Williams	UBV	205–207	2	40

2. Observations

High resolution optical spectroscopy for Doppler imaging was carried out at ESO during seven nights from May 18–23, 1996. The 1.4-m coudé auxiliary telescope (CAT) was used with the coudé echelle spectrograph (CES) in single-order mode. Together with the Loral 2688×512 15μ CCD the spectrograph provided a resolving power of 70,000 (3 $km\,s^{-1}$) in a useful wavelength range of around 70 Å. All integrations were set at an exposure time of 20 min and have typical signal-to-noise ratios of 250:1 and were centered at 6425 Å. This sequence allowed for a reasonably good phase sampling with a total of 29 high-S/N spectra but has two 0.17-phase gaps near $0\overset{p}{.}2$ and $0\overset{p}{.}7$ due to bad weather.

Data reductions were done with IRAF and included bias subtraction, flat fielding and optimal aperture extraction. Forty flat-field exposures per night were averaged together and used to remove the pixel to pixel variation of the detector sensitivity. There is no obvious fringing on the CCD image at the wavelength of our observations. Frequent Th-Ar comparison spectra and spectra of a bright radial-velocity standard were obtained several times throughout the night to ensure an accurate wavelength calibration. Radial velocities were derived from cross correlating the V824 Ara spectra with the IAU velocity standard HR 4786 and are listed in Table 1.

Four sites provided us with contemporaneous broad-band photometry (Table 2, see also Dempsey et al. 1998). All data were taken differentially with respect to the comparison stars HD 156427 (K4-5III) and HD 154775 (K5-M0III). After excluding data from bad nights and grossly deviant points from the remaining nights the entire data set described in Table 2 shrunk to basically the SAAO data plus two nights from Mt. John University Observatory (MJUO) and one night from Auckland and Waiharara. However, wavelength dependent zero-point shifts with respect to the SAAO data were evident from the check-star and comparison-star magnitudes and have been corrected for by simply determining average check-minus-comparison magnitudes and shifting them to the respective SAAO values. The MJUO minus SAAO shifts were $-0\overset{m}{.}01$ in V, $+0\overset{m}{.}025$ in B-V, $-0\overset{m}{.}01$ in V-R, but inconsistent in U-B. The Auckland and Waiharara minus SAAO zero-point shifts were $-0\overset{m}{.}02$ in V, and also rather inconsistent in the U and B bandpasses so that we decided not to use them. The remaining data are plotted later in the light curve in Fig. 7.

Table 3. Improved orbital elements

Element (Unit)	Value
$P_{\rm orb}$ (days)	1.6816463±0.0000003
T_0 (HJD)	2446998.4102 (adopted)
γ (km s^{-1})	+5.9±0.2
K_1 (km s^{-1})	86.0±0.4
K_2 (km s^{-1})	94.6±0.7
e	0.0 (adopted)
$a_1 \sin i$ (km)	1.9889±0.0088 × 10^6
$a_2 \sin i$ (km)	2.1871±0.0165 × 10^6
$m_1 \sin^3 i$ ($M_\odot$)	0.539±0.006
$m_2 \sin^3 i$ ($M_\odot$)	0.490±0.005
RMS for solution (km s^{-1})	2.37

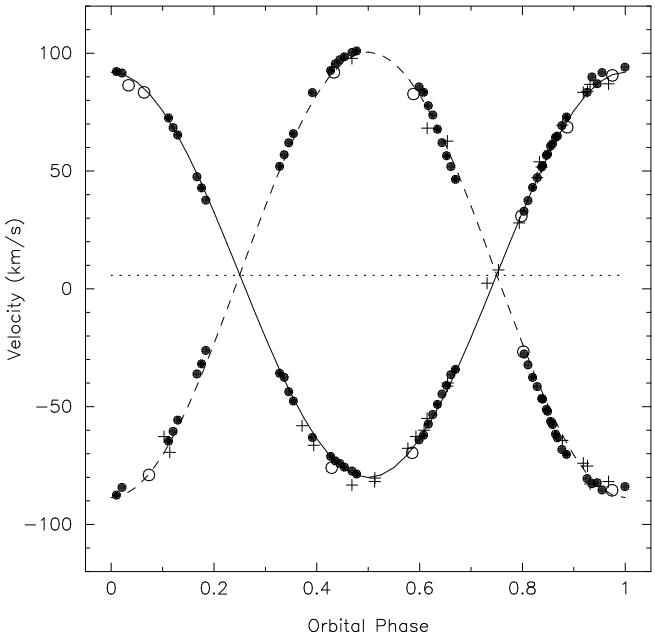

Fig. 1. Observed and computed radial velocity curves for the two components of V824 Ara. Dots are our new ESO measures from this paper, plusses are the photographic data of Bennett et al. (1962), and open circles are the ESO data of Pasquini et al. (1991).

3. Spectroscopic orbit and absolute dimensions

3.1. Orbital elements

A byproduct of the spectroscopic time series for Doppler imaging is the accurate measurement of radial velocities for both stellar components. We obtained altogether 94 new velocities (47 for each component) and use them to recompute the orbital elements of V824 Ara. We add the previously published ESO-CAT CCD velocities from Pasquini et al. (1991), taken between 1984–1990 (13 data points), and the original photographic data from Bennett et al. (1962), taken between 1959 and 1961 (32 data points). Our new velocities were obtained from cross correlations of the full V824 Ara spectrum with a spectrum of the IAU velocity standard β Crv = HR 4786 (G5IIb, $v_{\rm r} = -7.0$ km s^{-1}) and have external errors of 2.5 km s^{-1} for the primary and 2.7 km s^{-1} for the secondary. The velocities are listed in Table 1 along with their O–C's.

We decided to give all ESO-CAT CCD data unit weight while the older photographic data were given half weight. Final orbital elements were then derived with the updated differential-correction routine of Barker et al. (1967). A first run with the elements from Pasquini et al. (1991) already converged at an eccentricity so close to zero that a formal zero-eccentricity solution was adopted. The improved elements are listed in Table 3 and the computed velocity curves are plotted in Fig. 1 along with the observations.

Some of our orbital elements in Table 3 are significantly different than those presented by Pasquini et al. (1991) and leads to minimum masses for the two stellar components larger by about 10 %. This is mainly because our newer CCD data are of much higher precision than the photographic data of Bennett et al. (1962) that made up the bulk of velocities in the solution of Pasquini et al. (1991). No systematic zero-point shifts were apparent though.

All phases in this paper are computed with the new elements in Table 3.

3.2. Absolute dimensions and age

The major constraints come from the parallax measurement by the *Hipparcos* satellite (ESA 1997) that revised the distance of V824 Ara to 31.4±0.8 pc and thus $M_V = +4.34 \pm 0.05$ mag. This makes the two stars a factor of two fainter than previously thought. However, the absolute magnitude is not based on the brightest V-magnitude observed so far, i.e. V=6$^{\rm m}$.64 in 1984 (Cutispoto 1998). For V824 Ara we adopt a (combined) visual brightness of 6$^{\rm m}$.82 which is an average of the observed maximum brightnesses from the many sources cited in Cutispoto (1998). The peak magnitude in 1984 is too bright for the Hipparcos distance and the given spectral type by approximately 0$^{\rm m}$.1–0$^{\rm m}$.2. In fact, such brightening is likely due to plage activity that occurs simultaneous with cool spots. A recent Doppler image of the K0 giant XX Tri (HD 12545) revealed a large cool spot on one side of the star but also a large warm feature on the opposite side (Strassmeier 1999). This combination mimicked an intrinsically brighter star by about 0$^{\rm m}$.1–0$^{\rm m}$.2 than suggested from the effective temperature.

Together with the components' magnitude difference of 0$^{\rm m}$.87 measured from the equivalent-width ratio in the CORAVEL bandpass (Pasquini et al. 1991), we find the individual components' absolute magnitudes to be $M_V(S1) = +4^{\rm m}.73$ and $M_V(S2) = +5^{\rm m}.60$. The propagated error from the parallax and the brightness difference results in an uncertainty of just $\pm 0^{\rm m}.05$ for both components, but assumes no error for the apparent brightness adopted. If strictly on the main sequence, these magnitudes result in differences between the minimum masses and the canonical masses from, e.g., Gray (1992) of $\Delta m = 0.5$ and 0.4 solar masses for the two compo-

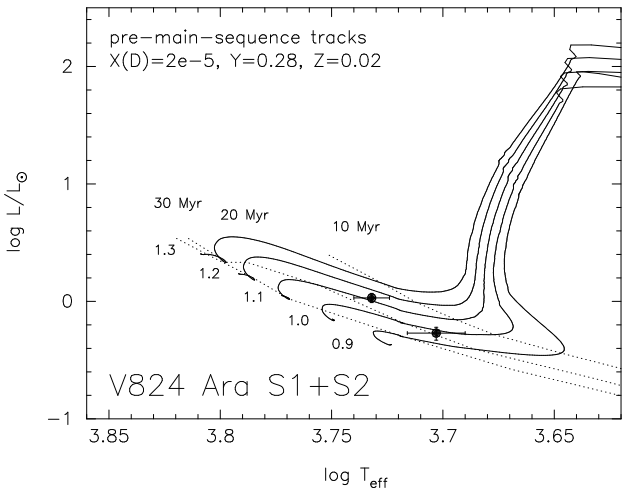

Fig. 2. The position of V824 Ara S1+S2 in the H-R diagram (primary: left dot; secondary: right dot). The solid lines are the pre-main-sequence tracks of D'Antona & Mazzitelli (1997) for masses of 0.9, 1.0, 1.1, 1.2, and 1.3 solar masses. The dotted lines are isochrones for 10, 20, and 30 Myr.

Table 4. Astrophysical data for V824 Ara a+b

Parameter	Value
Spectral type (star 1 + star 2)	G5 (IV) + K0 (IV-V)
Age	$\approx$ 18 Myr
$T_{\rm eff,1}$ (K)	5400±100
$T_{\rm eff,2}$ (K)	5050±150
$v_1 \sin i$ (km s^{-1})	36.8±1.0
$v_2 \sin i$ (km s^{-1})	33.7±1.5
$R_1 \sin i$ (R$_\odot$)	1.22
$R_2 \sin i$ (R$_\odot$)	1.12
Distance (pc)	31.4±0.8
$\log g_1$	4.0±0.5
$\log g_2$	4.5±0.5
$M_V(S1)$ (mag)	+4.73
$M_V(S2)$ (mag)	+5.60
L_1 (L$_\odot$)	1.07±0.05
L_2 (L$_\odot$)	0.535±0.025
Inclination	$52^\circ{}^{+10}_{-10}$
Masses with $i \equiv 52^\circ$ (see text):	
m_1 (G5 star)	1.101±0.013 M$_\odot$
m_2 (K0 star)	1.001±0.011 M$_\odot$

nents, respectively. If accounted for by the inclination angle i, it suggests an inclination of $54 \pm 1^\circ$. Since this is very close to our "best" value from the Doppler images, we may conclude that the two components are very close to the zero-age main sequence.

Both components' relatively high luminosities of 1.07 and 0.54 $L_\odot$ (obtained with the bolometric corrections from Flower 1996) and their high lithium abundances then suggest them to be in the process of just arriving on the ZAMS rather than leaving it. Fig. 2 shows the position of the two stellar components in the H-R diagram with respect to the pre-main-sequence tracks of D'Antona & Mazzitelli (1997). A formal comparison gives masses of 1.12 and 0.99 solar masses for the primary and secondary, respectively. However, as warned several times by D'Antona & Mazzitelli, such a straightforward comparison may not be conclusive because of the remaining theoretical uncertainties from the Deuterium-burning process and convection treatment. Nevertheless, if we adopt an inclination of 52° both "observed" masses in Table 3 and Table 4 agree to within their formal error bars with the masses from the evolutionary tracks in the H-R diagram. With this inclination the masses are also in agreement with the theoretical stellar models favored by Pasquini et al. (1991). The isochrone that fits both stars best suggests an age of ≈18 Myr for V824 Ara (Fig. 2).

For convenience, Table 4 summarizes the relevant stellar parameters for V824 Ara.

4. A Doppler image for May 1996

4.1. TempMap and binary-star spectrum synthesis

All Doppler maps in this paper were generated with the TEMPMAP code of Rice et al. (1989) described in Piskunov & Rice (1993) and most recently in Rice & Strassmeier (1998). It performs a maximum-entropy regularization for the inversion and includes a rigorous treatment of the local line profiles by synthesizing a small strip of spectrum around the main mapping line. A grid of model atmospheres with temperatures between $T_{\rm eff}$ = 3500 and 6000 K in steps of 250 K and fixed $\log g = 4.0$ for the primary and $\log g = 4.5$ for the secondary were taken from the ATLAS-9 CD (Kurucz 1993) and cover the expected surface temperatures on both components of V824 Ara. For each model atmosphere local line profiles were computed under the assumption of solar abundances with a wavelength spacing of 0.005 Å. This procedure ensures that blends from the same star are sufficiently resolved and included in the reconstruction process but can not treat the spectrum and continuum of the secondary star at the same time as the primary. Therefore, we solve for the two stellar components completely independently. Their relative contributions to the combined spectrum are predetermined from a spectrum synthesis with the program and technique described by Barden (1985). It involves a series of at least two MK standard-star spectra, obtained with the same equipment at ESO, that are rotationally broadened, shifted in radial velocity and in continuum intensity until they fit the observed spectrum of V824 Ara. In this way the relative continuum contributions were found to be 0.70±0.02 and 0.30±0.02 for the primary and secondary component, respectively, in very good agreement with earlier results by Pasquini et al. (1991) for the lithium-wavelength region at 6708 Å. We then multiply the normalized spectra with the appropriate contribution factors (1.30 and 1.70, respectively) to account for the presence of the two continua. Blended phases were excluded from the Doppler-imaging solution to avoid uncertainties due to blending. A more detailed description of the preparation of combined spectra for Doppler imaging was given recently in Strassmeier & Bartus (2000).

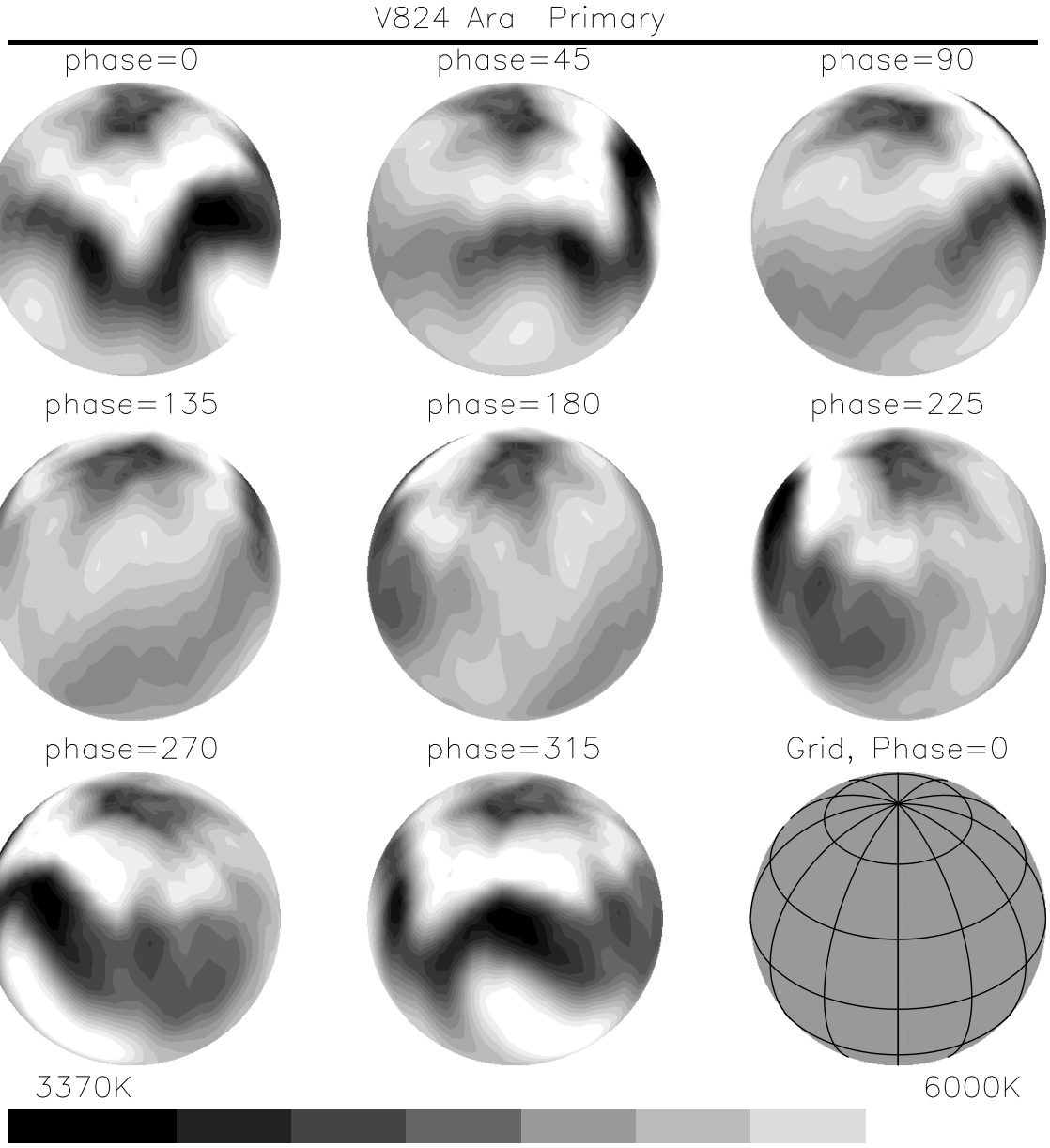

Fig. 3. a Doppler image of the primary of V824 Ara from Ca I 6439 Å. A spherical projection style at eight phases in steps of 45° (0.$^{\rm p}$25) is adopted. A dummy in the lower right corner shows the surface grid.

4.2. Adopted atomic line data, $v \sin i$, and effective temperatures

The broad lines of V824 Ara, combined with the limited wavelength coverage of our spectra, were such that we can use two spectral regions for mapping the primary component, i.e. Ca I 6439.075 and Fe I 6430.844, but only one for the secondary star (Ca I 6439 Å). The transition probabilities ($\log gf$ values) for these lines were adopted from a comparison of synthetic profiles with the respective solar lines and were obtained and discussed in previous papers in this series (e.g. Strassmeier et al. 1999). Preliminary stellar parameters for the two components were adopted from Pasquini et al. (1991) and from our new orbital elements and included the inclination of the rotational axes of around 50° and starting $v \sin i$ values of 37 km s^{-1} and 29 km s^{-1} for the G5-primary and K0-secondary, respectively. Surface temperatures of 5400 K (G5-star) and 5050 K (K0-star) were also adopted as starting values for the line-profile inversion. We note though that the line-profile inversion is independent of these starting values but approximately correct values help to achieve a solution more quickly.

4.3. Results

Fig. 3 and Fig. 4 show our Doppler images of V824 Ara. A representative spectrum is shown in Fig. 5a. These maps were derived with an inclination of 52° and $v \sin i$ of 36.8±1 km s^{-1} and 33.7±1.5 km s^{-1} for the primary and secondary com-

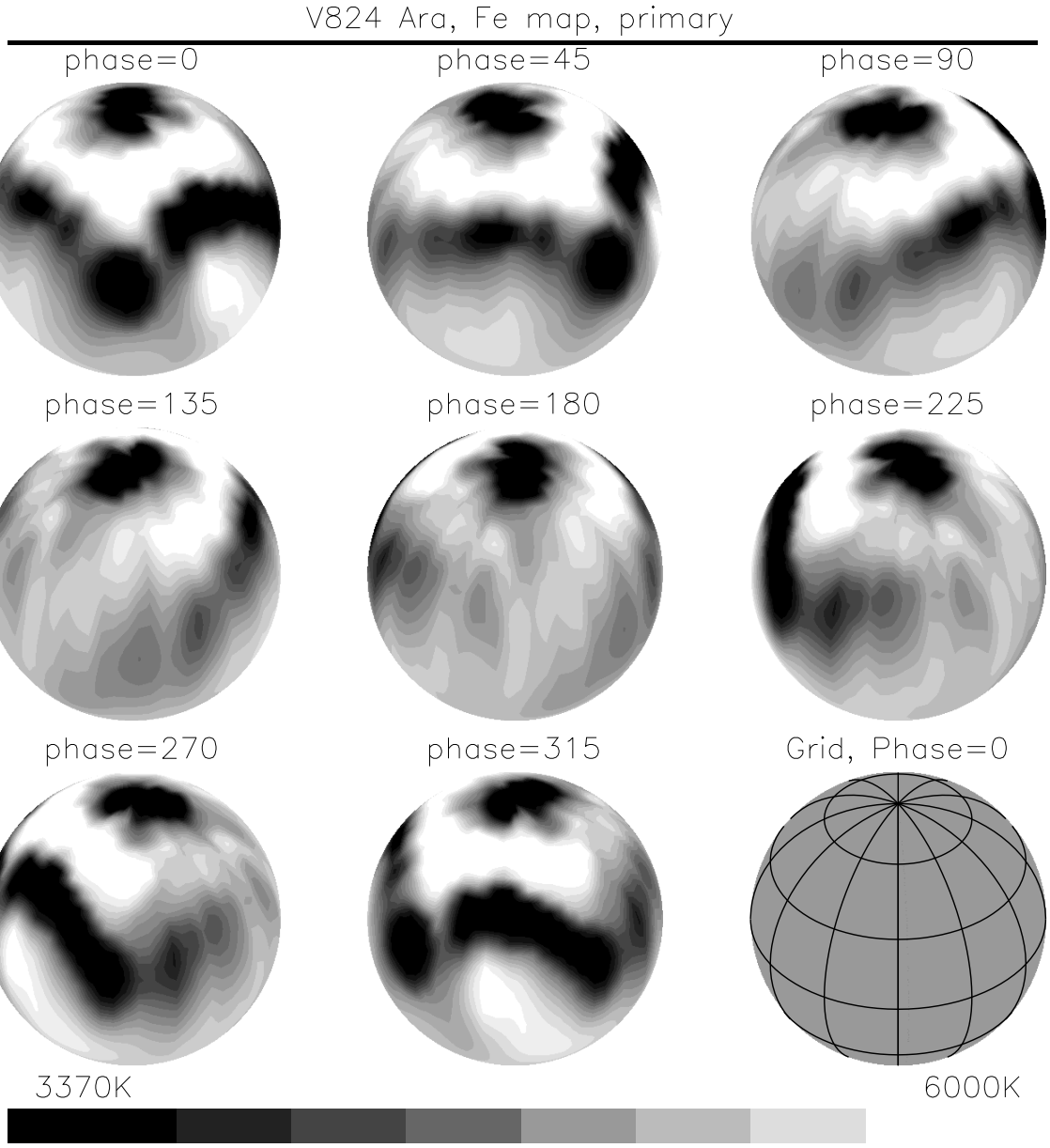

Fig. 3. b Doppler image of the primary of V824 Ara from Fe I 6430 Å.

ponent, respectively, and micro- and macroturbulences of 2.0 km s^{-1} with solar abundances. Figs. 5b,c show the observed calcium line profiles and the fits obtained from their inversion. The range of surface temperatures on the primary is 3400–6000 K with an average (surface-integrated) value of 4900 K while the secondary shows a range of 3300–6000 K and an average of 4550 K. The most significant feature on the primary is a complex equatorial region covering the longitudes between $\ell \approx 270°$ and about $\ell = 360°$. Its coolest part consists of a large, somewhat elongated spot tilted against the stellar equator and located at $\ell \approx 315°$. The photometric data in Fig. 7 show a corresponding sharp minimum at that phase ($\approx 0\overset{\text{p}}{.}8$) along with a broad maximum at around phase $0\overset{\text{p}}{.}0$–$0\overset{\text{p}}{.}1$ and is thus in qualitative agreement with the primary's spot distribution. Our primary-star maps also recover a cool and slightly asymmetric polar spot with a temperature difference of approximately 1700 K relative to the adopted "unspotted" photosphere of 5400 K. An appendage at $\ell \approx 180°$, that reaches down to approximately $+60°$ in latitude, is also evident and is recovered from both spectral regions. Its appearance in both maps in Fig. 3 is very similar except the contrast appears stronger in the Fe map. This is not as pronounced for the low-latitude spots and therefore we believe that the higher contrast is caused by the blending from the nearby Fe II 6432 line and is artificial. The local line profile of Fe II 6432 is not well determined due to uncertain damping coefficients in such singly ionized lines.

The secondary star does not show a polar cap-like spot but has instead a cool, very high-latitude spot at $\ell \approx 250°$ and $b \approx +70°$ that is probably connected with several lower latitude feature at around $\ell = 130 - 230°$. A very small and

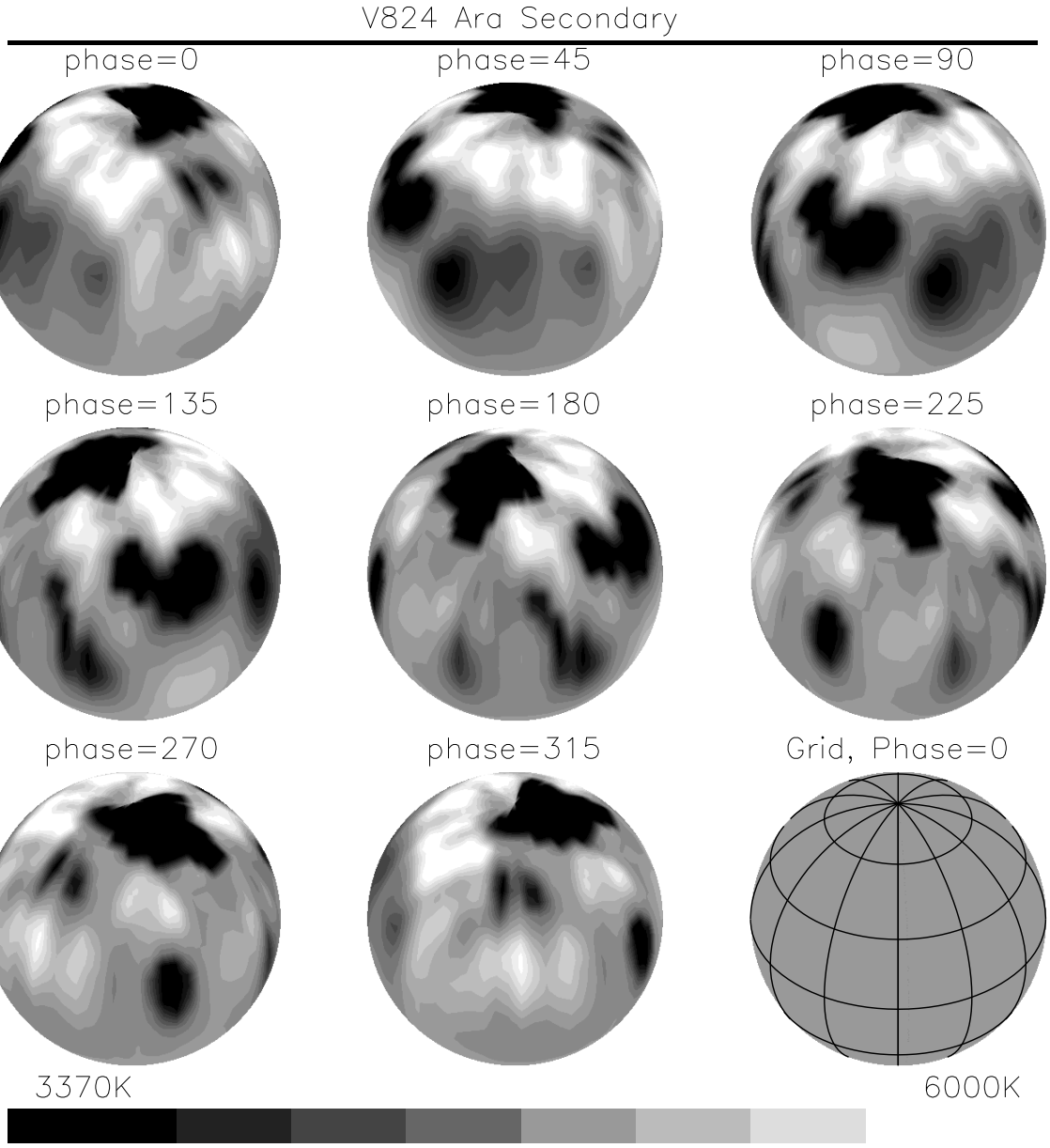

Fig. 4. Doppler image of the secondary component from Ca I 6439 Å. Otherwise as in Fig. 3. The Fe I 6430 line of the secondary is severely blended by the Fe II 6432 line from the primary and was therefore not used for Doppler imaging.

particularly cool feature at $\ell = 130°$ and $b \approx +30°$ with $\Delta T \approx 1800$ K is required by a sharp bump in the data at these phases, e.g. $0\overset{\text{P}}{.}330$ and $0\overset{\text{P}}{.}339$ in Fig. 5c. Its contrast could have been artificially enhanced by some subtle uncertainties due to the continuum subtraction of the primary. We have performed several tests by applying either excessive smoothing to the data prior to the inversion or different factors of relative continuum contribution. The feature, although persistent, did weaken in the extreme test cases which suggests that at least part of the profile bump is due to noise but certainly not all of it.

Because our data were phased with the orbital period and from a zero point at quadrature with the primary receded, the longitudes of 90° on the primary and 270° on the secondary are the facing hemisphere's central meridians. A comparison of our Doppler images in Fig. 3 and Fig. 4 does not show the main spot concentrations at these longitudes. Instead, the spots seem to group near 270° on the primary and 90° on the secondary, i.e. exactly the opposite distribution than that of the two polar spots seen by Hatzes & Kürster (1999) in 1990. The reversed spot concentration is also obvious from the predicted light curves in Fig. 7 where the primary shows its light minimum at phase $0\overset{\text{P}}{.}85$ and the secondary at $0\overset{\text{P}}{.}45$. However, we can fully confirm the finding by Hatzes & Kürster (1999) that the low-latitude spots on both V824 Ara components are preferentially located on the *anti-facing* hemispheres. Again, we emphasize that the spots on V824 Ara tend to be located preferentially along the apsidal line but on the hemispheres turned away from each other.

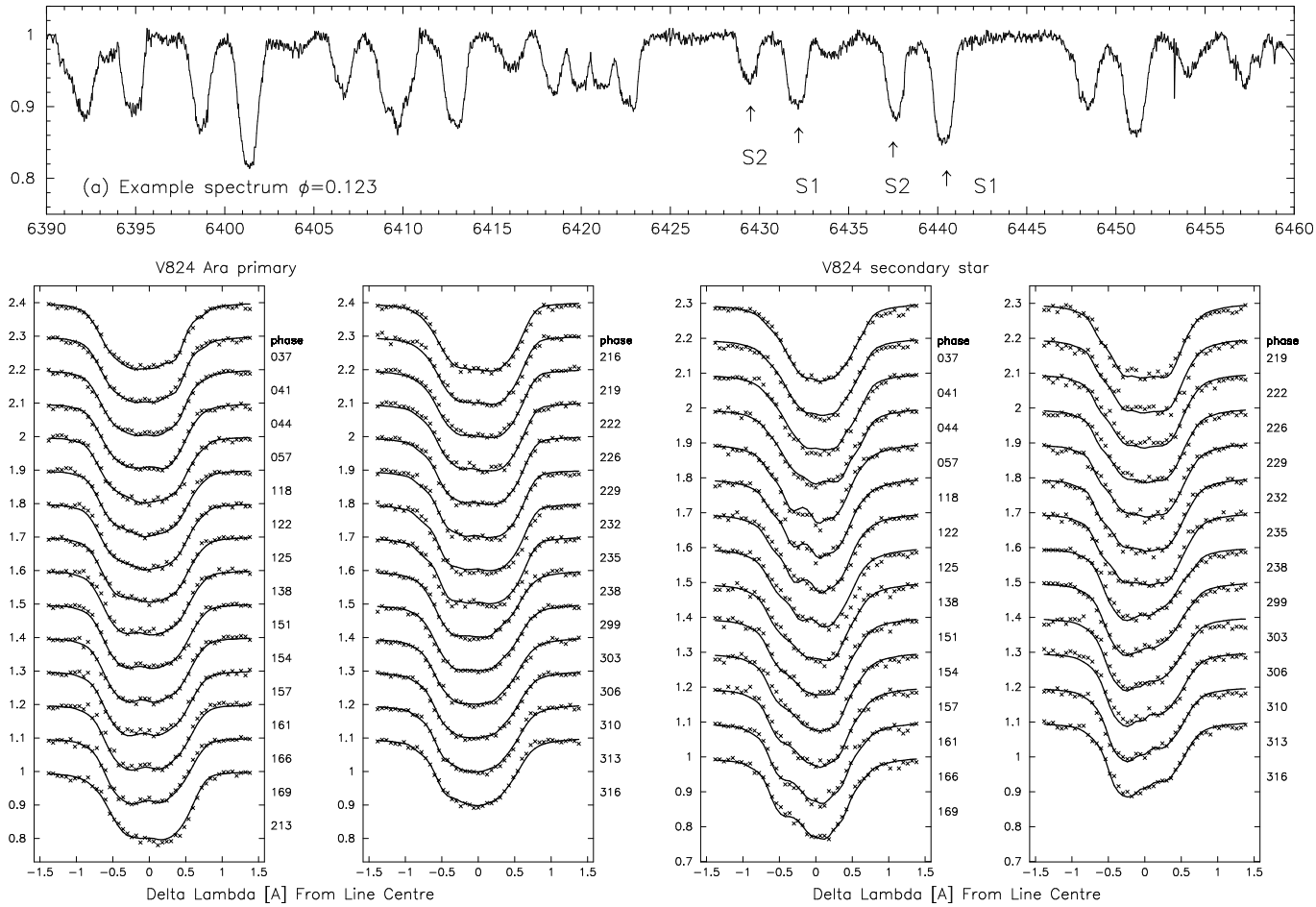

Fig. 5. a A representative plot of the combined V824 Ara spectrum and the identification of the Ca I 6439 Å and Fe I 6430 Å lines from both components (primary component =S1, secondary component =S2). **b,c** Observed and computed Ca I 6439 line profiles for both stellar components of V824 Ara Dots are the observations and lines are the fits from our Doppler images.

4.4. Coplanarity?

An uncertainty that remains with Doppler imaging of binary stars is the assumption that the inclinations of the rotational axes of the two binary components are indeed perpendicular to the orbital plane and parallel to each other. Zinnecker (priv. commun.) suggested to us that a misalignment would have a profound impact for the theory of binary-star formation in open clusters and that a very young binary system would be ideal to test such a hypothesis. For main-sequence and post-main-sequence binaries, it has been already argued that the asynchronuously rotating active components of the RS CVn- and BY Dra binaries may be a direct cause of a misalignment of their rotational axes (e.g. Glebocki & Stawikowski 1997).

V824 Ara is the only known (close) pre-main-sequence binary where both components can be Doppler imaged independently. It thus allows – at least in principle – the determination of the inclination for both components separately. From numerical inversions of artificial test data it was amply demonstrated that the misfit between the data and the model (χ^2) was minimized when the correct inclination is adopted (e.g. Kürster et al. 1994, and previous papers in this series). Fig. 6 shows the χ^2 distribution for the Doppler images of both components of V824 Ara for a large range of inclinations. Both distributions show a flat minimum of width ≈20° at about the same inclination range (42°–62° for the primary and 48°–68° for the secondary component, respectively). The formal values are found from a low-order polynomial fit to the χ^2 curves and are 52° for the primary and 58° for the secondary. However, note that the ranges of inclinations given are not error bars but simply state that inclinations within this range are equally likely. The quality and sampling of the present data limits the precision to which the inclination can be determined. We do not regard the formal difference of 6° as significant. Therefore, we conclude that the rotation axes of the two components are aligned and perpendicular with respect to the orbital plane and adopt 52° as the most likely inclination.

4.5. Predicted versus observed light and color curves

In case of a single star, or a single-lined spectroscopic binary, we usually also solve for the absolute continuum light in at least two photometric bandpasses simultaneously with the line profiles (usually Johnson-Cousins VR and VI because of the

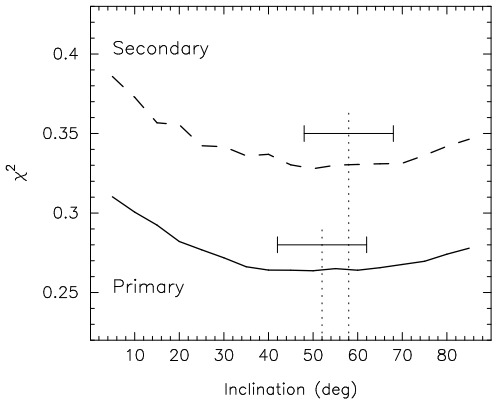

Fig. 6. The misfit between the data and the predicted profiles (χ^2) as a function of stellar inclination. The full line is for the primary (G5), the dashed line for the secondary (K0). The most likely values are indicated with a vertical dotted line, and the range of possible values is shown as horizontal bars. Note that both ranges significantly overlap, which suggests that the inclinations are very likely identical for both components.

larger spot contribution at longer wavelengths). However, in case of V824 Ara the light-curve variations are made up from the contributions from two stars because both components are active and covered with starspots. This makes the light-curve inversion relatively arbitrary and highly non-unique and we can not include the photometry in our image reconstruction star by star.

Instead, we compare the observed (combined) light curves with the predicted light and color curves obtained from the individual Doppler images. The average brightness in V is generated by fitting the flux of the continuum at 5500 Å for the Kurucz (1993) atmospheres to the standard values for the absolute magnitudes, $M_V(S1)$ and $M_V(S2)$, corrected for radius and gravity and then using the fits to these data to estimate the V magnitude for both spotted stars. These magnitudes agree reasonably well with the ones from the equivalent-width ratios (Sect. 3.2) and from the spectrum synthesis of the line strengths (Sect. 4.1) if the chemical abundances of calcium and iron are increased by 0.05 dex with respect to the Sun. We do not necessarily consider this increase as real because the absolute fluxes for pre-main-sequence stars likely deviate from the available standard model atmospheres. We then generate light variations in V and in each of B, R_C, and I_C by applying the calculated colours for B-V, V-R_C and V-I_C to the calculated V-light curves for both stars. Fig. 7 shows the observed and computed individual and combined light and color curves. Note that our photometry of V824 Ara was taken approximately two weeks prior to the spectroscopy and we can not be sure that the light-curve shape has not changed during that time. Cutispoto (1998) detected a full amplitude of less than $0\overset{\mathrm{m}}{.}04$ in 1992, while our data show an amplitude of $0\overset{\mathrm{m}}{.}1$. However, earlier photometry from Lloyd-Evans & Koen (1987) from sixty consecutive nights in 1981 indicated only small amplitude variations of the order of a few hundredth of a magnitude.

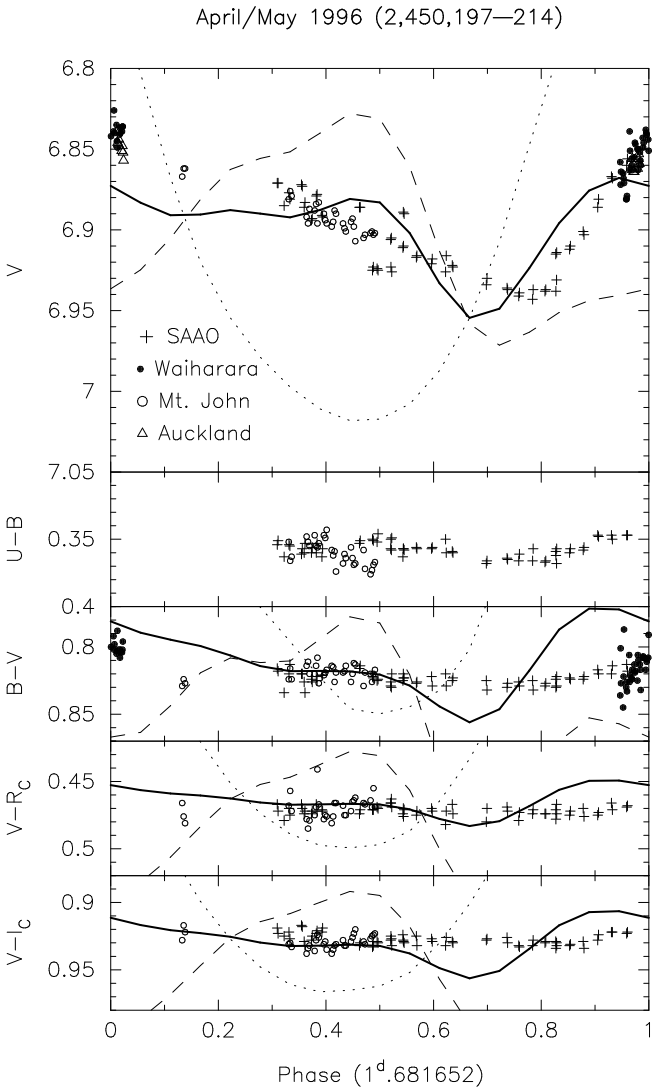

Fig. 7. Contemporaneous light and color curves of V824 Ara from April/May 1996. The V-light amplitude amounted to a full $0\overset{\mathrm{m}}{.}1$, while the color-curve modulations were only marginally detectable but suggest a weak minimum at the same phase as the V-light curve. The lines are the predicted (absolute) light and color curves from the Doppler images. Full line: both stars combined with $\Delta m = 0\overset{\mathrm{m}}{.}87$; dashed line: primary; dotted line: secondary. Note that the light and color curves of the individual stars were shifted vertically to show them in the viewport.

5. Discussion and conclusions

The existence of a polar or at least a very high-latitude spot together with large low-latitude features likely indicates a mixture of solar and non-solar magnetic flux behavior. Firstly, the Sun does not show a polar spot at all, secondly, it does not exhibit spots larger than a fraction of a percent of the visible hemisphere and, thirdly, spot occurence is limited to just a narrow equatorial band.

A peculiarity from our Doppler images is that the low-latitude spots on V824 Ara seem to be mostly concentrated on the hemispheres turned away from each other. Hatzes &

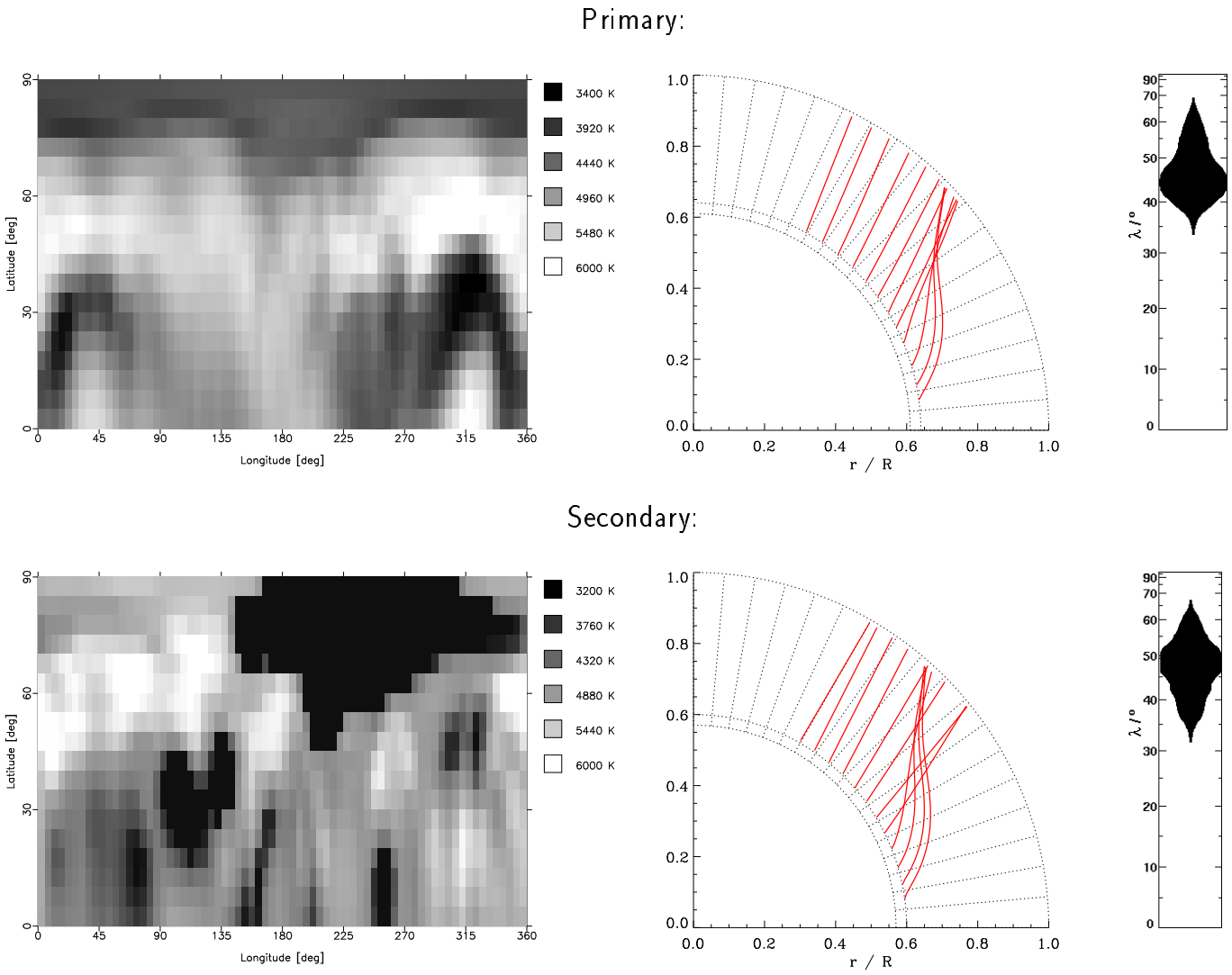

Fig. 8. The predicted latitude distribution of emerging flux tubes for the two stellar components of V824 Ara and a comparison with our Doppler images. The stellar models were computed from an updated version of the Kippenhahn-code (see Granzer et al. 1999) for pre-main-sequence models matching V824 Ara. A radial cross section (middle panels) is shown with the trajectories of the summit of rising flux loops. The small sector below the convection zone at $r/R \approx 0.6$ indicates the width of the overshoot region. The right panels show the spot-distribution probability on the stellar surface as a function of latitude (λ). Note that the predictions do not match the observations (see text).

Kürster (1999) had already noticed a symmetry of the spot distributions in their Doppler images from 1990 (i.e. their images look nearly identical if one reverses or flips one with respect to the other). Both component's polar spots were slightly decentered with respect to the stellar rotation pole and shifted in the direction of the other component. On the contrary, all low-latitude spots in both images from Hatzes & Kürster are located on the stellar hemispheres pointing away from each other. Hatzes & Kürster (1999) argued that the low-to-mid latitude spots represent artifacts due to mirroring with the decentered polar spot and did not further discuss their results. Our map of the secondary star does not show a cap-like polar spot – in agreement with the result of Hatzes & Kürster (1999) – but shows a high-latitude spot just touching the pole and several low-to-mid latitude features similar to the ones found by Hatzes & Kürster. We claim that a mirroring effect due to a polar spot does not affect the latitudes above the equator but just the regions that appear close to the "southern" stellar limb, i.e. usually the latitudes below the equator. Further agreement exists with the recovery of an asymmetric polar spot on the primary. But again, the asymmetry we detected (i.e. the appendage in the top map in Fig. 8) is not pointing toward the secondary star but instead 90° perpendicular to it in the direction of the orbital motion. Since there is no obvious reason that either ours or Hatzes & Kürster's images are wrong, we conclude that the surface spot distribution on V824 Ara may undergo a systematic, and possibly even cyclic, variation. Just recently, Berdyugina et al. (1999) found such a cyclic "flip-flop" behavior on the RS CVn binary II Peg from six consecutive years of Doppler imaging. They found that during that time only two (active)

longitudes with a separation of 180° were occupied by spots and that the spot area evolved alternately, i.e. if one spot or spot group got larger, the other one got smaller. The time scale of this "flip-flop" was approximately four years.

A latitudinal bimodality of the spot distribution was recently predicted for very young pre-main-sequence stars from flux-tube modelling (Granzer et al. 2000). To investigate the theoretically expected spot distribution for V824 Ara, we adopt the MHD code used by Granzer et al. (2000) – originally designed by Caligari et al. (1995) and Schüssler et al. (1996) – in combination with a model of the solar convection zone as an approximation to V824 Ara and spin it up to the rotation period of V824 Ara ($\Omega = 16\,\Omega_\odot$). Two underlying stellar pre-main-sequence models are computed matching the masses of the two components of V824 Ara, i.e. 1.1 and 1.0 $M_\odot$ for the primary and secondary, respectively. Both models were computed with a mixing-length parameter, $\alpha = \ell/H_p$, of 1.67. Hydrogen burning was assumed to contribute 0.01% of the total luminosity according to a nominal age of ≈18 Myr.

The result of these calculations is shown in Fig. 8 in form of a stellar crossection and a surface spot-probability function for each stellar component. The crossections show the path of the crests of the emerging flux tubes plotted as lines. The spot-probability pattern is shown as a function of latitude. A larger width of the pattern corresponds to a higher probability of emerging magnetic flux. The two main features from this figure are, first, we would expect to see magnetic flux only above a latitude of approximately 35–40° and no spots below that latitude, i.e., near the equator (for both stars). Second, if there is indeed a polar spot on the primary and a high-latitude feature on the secondary, parts of them must have formed after flux-tube emergence because the current model suggests no flux tubes at latitudes above 70°. A possible mechanism to transport flux to the pole is meridional circulation. Recent time-series Doppler images of the RS CVn binary HR 1099 suggest such a poleward migration scenario for this K0 subgiant (Vogt et al. 1999, Strassmeier & Bartus 2000) and would be also a possible explanation for the polar activity on V824 Ara. If such a meridional flow is coupled to the orbital motion, e.g. through the gravitational quadrupole moment as described by Lanza & Rodonó (1999) to explain the alternating orbital-period variations in active binaries, it would also present a possible explanation for the tendency of spots to group at preferred longitudes.

Our finding of similar or, very likely, identical inclinations for the two component's rotational axes is hampered by a large range of equally likely inclinations. At the moment it does not permit a more firm conclusion other than that the rotation axis of both components are most likely coaligned. Clearly, higher quality data and still better sampling is required. Nevertheless, V824 Ara is an excellent target for detecting a small misalignment if it exists.

Acknowledgements. KGS is very grateful to the Austrian Science Foundation (FWF) for support under grants S7301-AST (APT) and S7302-AST (Doppler imaging). JBR acknowledges support from the Natural Science and Engineering Research Council of Canada (NSERC). We thank Th. Granzer for computing the MHD flux-tube models for us and Dr. Y. C. Unruh for reading the manuscript. We also thank M. Kürster for his help with the remote-control observations at ESO in Garching in 1996.

References

Barden S. C., 1985, ApJ 295, 162
Barker E. S., Evans D. S., Laing J. D., 1967, ROB No. 130
Barnes J. R., Collier Cameron A., Unruh Y. C., Donati J.-F., Hussain G. A. J., 1998, MNRAS 299, 904
Bennett N. N., Evans D. S., Laing J. D., 1962, Roy. Obs. Bull., No. 61
Berdyugina S. V., Berdyugin A. V., Ilyin I., Tuominen I., 1999, A&A 350, 626
Caligari P., Moreno-Insertis F., Schüssler M., 1995, ApJ 441, 886
Collier Cameron A., 1995, MNRAS 275, 534
Cutispoto G., 1998, A&AS 131, 321
D'Antona F., Mazzitelli I., 1997, in Pallavicini R. & G. Micela (eds.), *Cool stars in clusters and associations*, Mem.S.A.It. 68, p. 807
Dempsey R. C., Linsky J. L., Schmitt J. H. M. M., Fleming T. A., 1993, ApJS 86, 599
Dempsey R. C., Neff J. E., Strassmeier K. G., Airapetian V. S., Lim J., 1998, in Donahue R. A. & J. Bookbinder, Cool Stars, Stellar Systems, and the Sun, PASPC 154, CD-1402
Dempsey R. C., Neff J. E., Airapetian V. S., Lim J., Linsky J. L., 2000, ApJ, in preparation
Donati J. F., 1999, MNRAS 302, 457
ESA 1997, The Hipparcos and Tycho catalog, ESA SP-1200
Flower P. J., 1996, ApJ 469, 355
Glebocki R., Stawikowski A., 1997, A&A 328, 579
Granzer Th., Schüssler M., Caligari P., Strassmeier K. G., 2000, A&A, in press
Gray D. F., 1992, in *The observation and analysis of stellar photospheres*, CUP, Cambridge
Hatzes A. P., 1995, ApJ 451, 784
Hatzes A. P., Kürster M., 1999, A&A 346, 432
Johns-Krull C. M., Hatzes A. P., 1997, ApJ 487, 896
Joncour I., Bertout C., Bouvier J., 1994, A&A 291, L19
Kürster M., Hatzes A. P., Pallavicini R., Randich S., 1992, in Giampapa M. S. & J. A. Bookbinder (eds.), $7th$ Cambridge Workshop on *Cool Stars, Stellar Systems, and the Sun*, PASPC 26, p. 249
Kürster M., Schmitt J. H. M. M., Cutispoto G., 1994, A&A 289, 899
Kurucz R. L., 1993, ATLAS-9, CD-ROM #13
Lanza A. F., Rodonó M., 1999, A&A 349, 887
Lloyd-Evans T., Koen M. C. J., 1987, SAAO Circ. 11, 21
Martin E. L., Brandner W., 1995, A&A 294, 744
Pasquini L., Cutispoto G., Gratton R., Mayor M., 1991, A&A 248, 72
Piskunov N. E., Rice J. B., 1993, PASP 105, 1415
Rice J. B., Strassmeier K. G., 1996, A&A 316, 164 (paper II)
Rice J. B., Strassmeier K. G., 1998, A&A 336, 972 (paper VII)
Rice J. B., Wehlau W. H., Khokhlova V. L., 1989, A&A 208, 179
Schüssler M., Caligari P., Ferriz-Mas A., Solanki S. K., Stix M., 1996, A&A 314, 503
Stout-Batalha N. M., Vogt S. S., 1999, ApJS 123, 251
Strassmeier K. G., 1999, A&A 347, 225 (paper XI)
Strassmeier K. G., Bartus J., 2000, A&A, in press (paper XII)
Strassmeier K. G., Hall D. S., Fekel F. C., Scheck M., 1993, A&AS 100, 173
Strassmeier K. G., Lupinek S., Dempsey R. C., Rice J. B., 1999, A&A 347, 212 (paper X)
Strassmeier K. G., Rice J. B., 1998, A&A 339, 497 (paper IX)
Strassmeier K. G., Rice J. B., Wehlau W. H., et al. 1991, A&A 247, 130
Vogt S. S., Hatzes A. P., Misch A., Kürster M., 1999, ApJS 121, 547